Journal of Constructional Steel Research 183 (2021) 106707

Contents lists available at ScienceDirect

Journal of Constructional Steel Research

Material pre-straining effects on fatigue behaviour of S355 structural steel

Satya Anandavijayan [a], Ali Mehmanparast [a,*], Jarryd Braithwaite [a], Feargal Brennan [b], Amir Chahardehi [c]

[a] Offshore Renewable Energy Engineering Centre, Cranfield University, Bedfordshire MK43 0AL, UK
[b] Naval Architecture and Marine Engineering, University of Strathclyde, G4 0LZ, UK
[c] Atkins Energy, Nova North, 11 Bressenden Pl, Westminster, London SW1E 5BY, UK

ARTICLE INFO

Article history:
Received 21 December 2020
Received in revised form 7 April 2021
Accepted 15 April 2021
Available online xxxx

Keywords:
Fatigue
S355
Offshore wind
Material pre-straining
S-N curve
Monopile

ABSTRACT

A commonly used material in offshore structures is S355 structural steel. For example, during the monopile fabrication process, the material is pre-strained to different levels at different depths through the thickness. Therefore, the influence of pre-straining on fatigue life and crack growth behaviour of the material needs to be examined and considered for design and life assessment procedures. In the present study, uniaxial fatigue and fatigue crack growth tests have been conducted on materials with different pre-strain levels and the results are compared with the un-strained material state. From the test data, it has been seen that the S-N fatigue life will reduce with increasing pre-straining level, while the fatigue crack propagation rate remains largely unchanged in pre-strained material. The results from this study are compared with the recommended S-N fatigue and fatigue crack growth trends available in standards and are discussed in terms of the applicability and level of conservatism in the recommended curves to account for the material pre-straining effects on the fatigue life assessment of offshore structures.

1. Introduction

There is a push for offshore wind which has resulted in the offshore wind industry developing newer technologies and install more wind farms with turbines of higher capacities in deeper waters [1]. Among different components of offshore wind turbines, foundation structures hold a significant importance in the future development of offshore wind project due to the significant costs involved in fabrication and maintenance of these assets [2,3,4,5]. Over the last decade, monopile foundation structures have been extensively utilised by offshore wind developers due to their simplistic design, production, and unit cost [6,7]. Monopiles currently account for over 80% of installed offshore wind turbines [6,7]. Therefore, the focus of this study is on the effect of manufacturing processes on the structural integrity of monopile structures. Separate studies must be conducted in the future to investigate the manufacturing defects on the design and integrity assessment of alternative types of offshore wind foundations including jackets.

Monopiles are fabricated via the three roll bending process, a continuous manufacturing process involving cold rolling of previously hot rolled structural steel plates into cylindrical cans, prior to being longitudinally welded. These cans are then welded together circumferentially to achieve the length of monopile required. In order to cold roll structural steel plates into curved shapes, they must be plastically deformed. From previous works it has been seen that the monopile fabrication process may result in plastic strains ranging from compressive on the inner surface of the steel plates to tensile on the outer surface, and the exact values vary through the thickness [8,9]. Studies have shown that introducing plasticity into metals during fabrication processes can affect the mechanical characteristics of the material [10,11]. Thus, in the case of monopile structures this is an important area that needs to be investigated to ensure accurate lifetimes are predicted using appropriate structural integrity assessment procedures.

Structural steels are widely employed in the fabrication of offshore structures due to their good strength characteristics, as well as good welding properties and ductility. While previous research works have extensively investigated the mechanical and fatigue behaviour of various grades of structural steels [12,13,14] the material pre-straining effects induced during the fabrication processes have not been examined yet. Work has been previously done to investigate the effect of hardening behaviour on the strength of S355. In the work by de Jesus et al. [15], monotonic stress-strain curves were obtained on S355 structural steel to evaluate the initial strain hardening behaviour of the parent material. It was observed from these results that S355 had a tensile strength between 470 and 630 MPa, for specimen thicknesses below 16 mm, with a yield plateau followed by significant strain hardening [15]. In the work by Forni et al. it was shown that S355 steel retains its strain hardening capacity with increasing strain rate, and at

* Corresponding author.
E-mail address: a.mehmanparast@cranfield.ac.uk (A. Mehmanparast).

https://doi.org/10.1016/j.jcsr.2021.106707

Nomenclature

a	Crack length
a_0	Initial crack length
a_f	Final crack length
B	C(T) specimen thickness
B_n	Net thickness between the side grooves
d	C(T) specimen hole diameter
D	Fatigue damage
E	Elastic Young's modulus
f	Frequency
H	C(T) specimen height
K_{max}	Stress intensity factor at maximum load
K_{min}	Stress intensity factor at minimum load
ΔK	Stress intensity factor range
N	Number of fatigue cycles
N_f	Number of cycles to failure in uniaxial fatigue tests
P_{max}	Maximum Load
P_{min}	Minimum Load
R	Load ratio in fatigue tests (P_{max}/P_{min})
W	C(T) specimen width
Y	Shape function
$\Delta\sigma$	Stress range
σ_{UTS}	Ultimate tensile stress
σ_{max}	Maximum stress
σ_{min}	Minimum stress
σ_y	Yield stress
ε_f	Tensile strain at failure
ε_p	Plastic strain

higher strain rates, an instability (such as lower and upper yield strengths) can be present due to the dislocation density, velocity, and loading rate [16, 17].

Another study was conducted on 430 stainless steel to explore the influence of material pre-strain on the fatigue behaviour. The test specimens were initially pre-tensioned to 5%, 8% and 12% strain and subsequently tested under fatigue loading conditions. From this work, it was observed that the tensile pre-straining resulted in a decrease in the number of cycles to failure, at the same stress range [19]. The fatigue behaviour of pre-strained 304 L steel was investigated and compared to the as-received materials in [20], and it was noted that pre-strained test specimens had shorter fatigue lives due to their decreased ductility after pre-straining. In a work by Hagiwara et al. [18], a comprehensive study was conducted on line pipe steels to compare the fatigue crack growth rates for various grades of steel, in the presence of pre-strains up to 20%. The results from this study showed that tensile pre-strain had no significant effect on fatigue crack initiation and growth behaviour of the materials tested [18].

While the fatigue design curves such as DNVGL-RP-C203 and life assessment procedures are primarily focussed on engineering materials without any pre-straining history, the results available in the literature suggest that the pre-straining effects on the fatigue life of steels must be carefully investigated and considered in the life assessment of offshore structures. In order to better understand the influence of pre-strains introduced during fabrication of offshore structures, the present study extensively investigates the fatigue life and crack growth behaviour in the presence of different levels of tensile pre-strains in S355 structural steel, which is widely used in fabrication of offshore wind turbine foundations, and the results are compared with the as-received material. The results are discussed in terms of the significance of pre-straining effects on design and life assessment of offshore wind turbine monopile foundations, and provide new insights to enhance the life prediction of the offshore structures.

2. Material pre-conditioning and specimen preparation

The material used in this research is S355GS + 10 structural steel due to its wide use in the manufacture of offshore structures. This material is known to have high ductility, allowing it to undergo large deformations [21,22]. In order to investigate the influence of material pre-straining on the fatigue properties of S355, the material was pre-strained to various levels of plastic strain. The three pre-straining conditions which were examined in this study were (1) base metal (BM) which is also known as the as-received (AR) material with 0% plastic strain, (2) uniformly pre-tensioned material to 5% plastic strain, and (3) uniformly pre-tensioned material to 10% plastic strain. The mechanical response of the AR material was preliminarily examined by performing an interrupted tensile test on an AR sample and the stress levels corresponding to 5% and 10% plastic strain, ε_p, were identified and applied in uniform pre-tensioning of the AR blocks of S355 in order to introduce the target values of pre-strains in the test specimens.

Subsequent to pre-tensioning of large blocks of S355 steel to 5% and 10% plastic strain, dog-bone shape specimens were extracted for tensile and uniaxial fatigue tests as well as compact tension, C(T), specimens for fatigue crack growth tests. Similarly, dog-bone and C(T) specimens were extracted from an AR block of S355 steel in order to prepare specimens with 0% plastic strain for testing and comparison with the pre-strained specimens. The dog-bone shape specimens for uniaxial fatigue tests were designed following the guidelines provided in ASTM E466 [23] and had the width of 24 mm, thickness of 11 mm and gauge length of 48 mm. The C(T) specimens for fatigue crack growth tests were designed in accordance with ASTM E647 [23], and had the total width of $W = 50$ mm, height of $H = 60$ mm, thickness of $B = 15$ mm, pin hole diameter of $d = 12.5$ mm and initial crack length of $a_0 = 22.5$ mm. All C(T) specimens were side grooved by 15% of the total thickness on each side and had the net-thickness between the side grooves of $B_n = 10.5$ mm.

3. Testing methodology

Uniaxial tensile and fatigue tests on dog-bone shape specimens were performed on a servo-hydraulic machine with load carrying capacity of 250 kN. To compare the mechanical behaviour of pre-strained materials, two tensile tests per pre-strain levels of 0%, 5% and 10% were performed on dog-bone shape specimens. For the uniaxial fatigue tests, alignment checks were made during the set-up and operation of tests by attaching strain gauges to the opposite sides of the test specimens. All uniaxial fatigue tests were performed under load control mode by implementing the maximum load, P_{max}, and minimum load, P_{min}, in a sinusoidal cyclic waveform. Uniaxial fatigue tests were performed at room temperature in air under a constant frequency of $f = 4$ Hz with the load ratio of $R = 0.1$. The uniaxial fatigue samples were continuously cycled, without any interruption throughout the test, until failure. The tests were performed at different values of stress range, $\Delta\sigma$, (described as the difference between maximum applied stress σ_{max} and minimum applied stress σ_{min}) and the number of cycles to failure, N_f, was recorded at the end of each test. In total, six AR, five 5% pre-strained and seven 10% pre-strained dog-bone shape specimens were tested under uniaxial fatigue loading conditions to investigate the influence of material pre-straining on the fatigue life of S355 steel. Moreover, additional fatigue tests were performed and interrupted before final failure, and were subsequently tested under monotonic loading to investigate the influence of cyclic loading history on the mechanical response of S355 materials with different pre-strain levels.

Fatigue crack growth tests on C(T) specimens were performed on a servo-hydraulic machine with loading capacity of 100 kN. The crack growth monitoring in these tests was conducted using the unloading compliance technique by attaching a clip gauge, with the maximum

travel range of 4 mm, at the crack mouth of the specimens. For this purpose, knife edges were machined on C(T) specimens to securely accommodate the clip gauge during fatigue crack growth tests. In addition to unloading compliance measurements, high resolution cameras were located behind and in front of the machine to compare the visually observed crack lengths at the free surfaces of C(T) specimens with those estimated from the unloading data. All fatigue crack growth test specimens were at room temperature in air under the frequency of $f = 2$ Hz and load ratio of $R = 0.1$. In total, three AR, four 5% pre-strained and four 10% pre-strained C(T) specimens were tested in this study to investigate the influence of material pre-straining on the fatigue crack growth behaviour of S355 steel.

Post testing, specimens were soaked in liquid nitrogen for ten minutes and then broken open under monotonic loading conditions. High resolution macroscopic images of the fracture surfaces were taken and analysed to measure the average fatigue crack growth in each test specimen. The estimated crack lengths from the unloading compliance were compared to the measured values obtained from the fracture surface to check the accuracy of the crack length estimates. As reported in Section 4, the percentage of error in crack length estimations from the unloading compliance data at the end of the fatigue growth tests, a_f, are below 7%, confirming that relatively accurate values of crack length were estimated using the clip gauge data.

4. Tensile and fatigue test results

4.1. Tensile tests

Tensile tests were conducted on 0%, 5% and 10% pre-strained specimens. Two specimens were tested per pre-straining level; denoted T-0%-1 and T-0%-2, T-5%-1 and T-5%-2, and T-10%-1 and T-10%-2, for 0%, 5% and 10% pre-strain levels, respectively. The Digital Imaging Correlation (DIC) technique was employed to accurately determine the strain distributions during tensile tests. An example of the DIC strain maps captured on specimens with 0%, 5% and 10% pre-strains at the given stress level of 480 MPa is shown in Fig. 1. As seen in this figure, before reaching the onset of plasticity the strains were uniformly distributed across the gauge region of the test specimens. The colour scales presented represent the axial strain along the loading direction when the specimen is held in tension at 480 MPa. In Fig. 1 the high and low strain regions are shown in red and dark blue, respectively. The strain values shown in Fig. 1 have the unit of $1/10^{-3}$ (strain/mstrain). It is worth noting that to plot the tensile curves, the average strain values were taken from an area in the vicinity of the necking and failure region for all the tensile tests performed in this study. As seen in Fig. 1 at a given stress level the pre-strained specimens display a lower % strain than AR specimens due to the hardening behaviour that occurs as a result of material pre-straining.

The average values of elastic Young's modulus, E, yield stress, σ_y, ultimate tensile strength, σ_{UTS}, and strain at failure, ε_f, from the two tests performed on each material pre-strain level are reported in Table 1 and the tensile curves are graphically presented in Fig. 2. From the table it can be seen that E, σ_y and σ_{UTS} exhibit an increase by increasing the pre-strain level, while the strain at failure continuously decreases. It is evident from these results that the rate of change in the yield stress of the material, as a result of pre-straining, is greater than that observed in σ_{UTS}.

4.2. Uniaxial fatigue tests

Uniaxial fatigue tests were performed on dog-bone specimens with 0%, 5% and 10% pre-strain (see Fig. 3). Due to relatively high ductility of S355, initial tests were performed at stress levels of above or close to the yield stress of the AR material and then the stress level was gradually decreased for the following tests via the staircase method. The stress range, $\Delta\sigma$, values applied in uniaxial fatigue tests were 430, 418, 406,

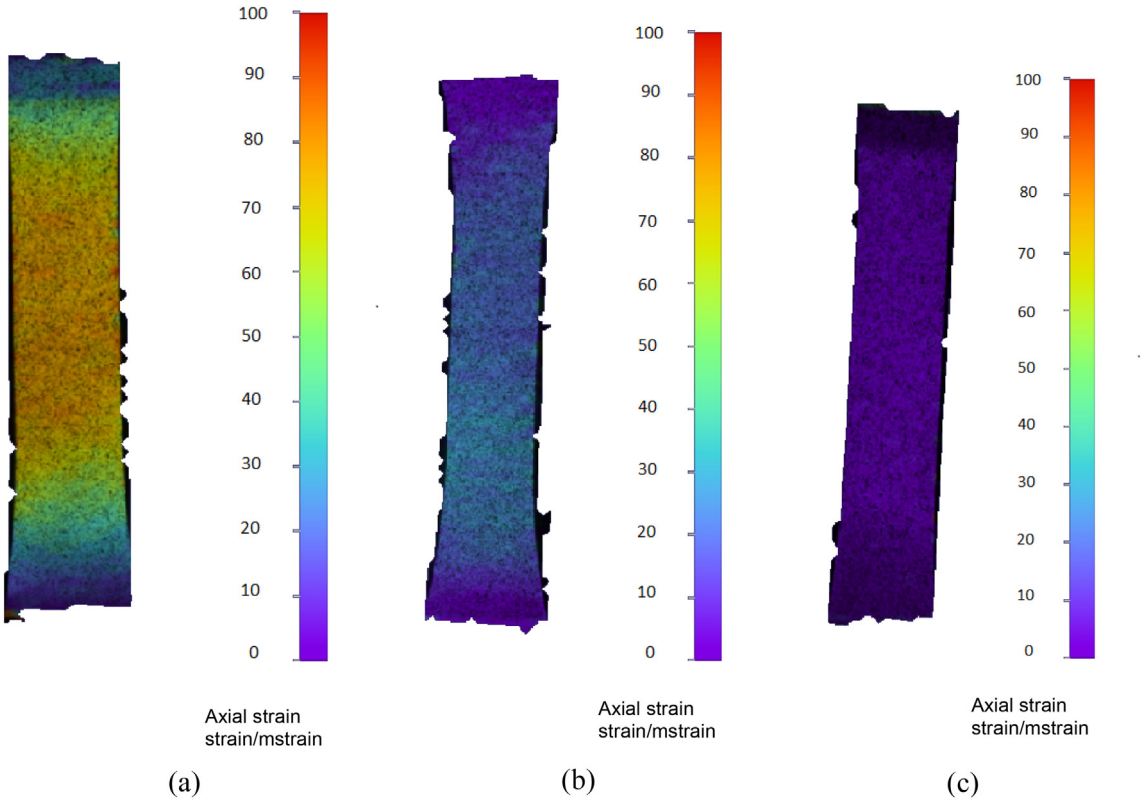

Fig. 1. DIC strain maps at 480 MPa for (a) 0%, (b) 5%, (c) 10% pre-strained specimens.

Table 1
Average mechanical properties for 0%, 5% and 10% pre-strained materials.

Pre-strain level (%)	E (GPa)	σ_Y (MPa)	σ_{UTS} (MPa)	ε_f (%)
0	222	417	517	50.8
5	255	468	532	49.0
10	264	516	545	46.6

400 and 391 MPa. The number of cycles to failure obtained from uniaxial fatigue tests are correlated with the applied stress range in Log-Log axes and the indicative S-N curves for different pre-strain levels are presented in Fig. 4. It can be seen in this figure that the number of cycles to failure seem to converge at high stress range values. The reducing fatigue life trend, compared to the AR material, can be consistently observed in 5% and 10% pre-strained data points, indicating that an increase in the pre-strain level decreases the fatigue life of the material.

Also seen in Fig. 4 is that for 0% (i.e. AR) and 5% material states, a sudden change in the slope of the S-N curve would occur at lower stress range values resulting in bi-linear trends, in Log-Log axes, for these two data sets. Moreover, interestingly the change of the slope in the S-N curves on both material data sets has been observed to happen around $N_f = 600{,}000$ cycles. For clarity, the data points at higher and lower stress range values with different slopes are shown in solid and hollow symbols, respectively, in Fig. 4. It is evident from the test results that the $\Delta\sigma$ at which the change in the slope of the S-N curves takes place decreases by increasing the pre-strain level. These results suggest that if the tests on 10% material were continued at lower $\Delta\sigma$, the same change in the slope would have also occurred in that material state.

In order to describe the fatigue life of examined tests specimens, the lines of best fit have been made to each data set to obtain the power-law constants correlating the stress range with the number of cycles to failure, in the form of the Basquin relationship which is described as:

$$N_f = A(\Delta\sigma)^B \tag{1}$$

The $\Delta\sigma$ exponents at high and low stress values are referred to as B_1 (with the corresponding $\Delta\sigma$ coefficient of A_1) and B_2, (with the corresponding $\Delta\sigma$ coefficient of A_2) respectively, and summarised in Table 2. It can be seen in this table that the magnitude of both B_1 and B_2 decreases by increasing the pre-strain level, with a higher rate of change observed in B_1 compared to B_2. Also seen in Fig. 4 and Table 2 is that while the magnitude of B_1 values for 5% and 10% pre-strain data sets have been found to be lower than the 0% data set, more tests need to be conducted in future work on 5% pre-strained material to quantify a more accurate slope with greater number of data points (the current B_1 calculation for 5% pre-strained material is only based on two data points). Comparing the obtained data on materials with different pre-strain levels presented in Fig. 4 and Table 2, an important conclusion derived from this study is that for a given stress range value, severe material pre-straining of up to 10% can reduce the fatigue life by more than an order of magnitude, compared to the AR material with 0% pre-strain level, and this difference in fatigue lives would increase at lower stress levels; however, further work needs to be conducted to confirm the fatigue behaviour at lower stresses. These results clearly demonstrate that material pre-straining has a detrimental effect on fatigue life and this effect potentially may be more pronounced at lower stresses and higher pre-strain levels.

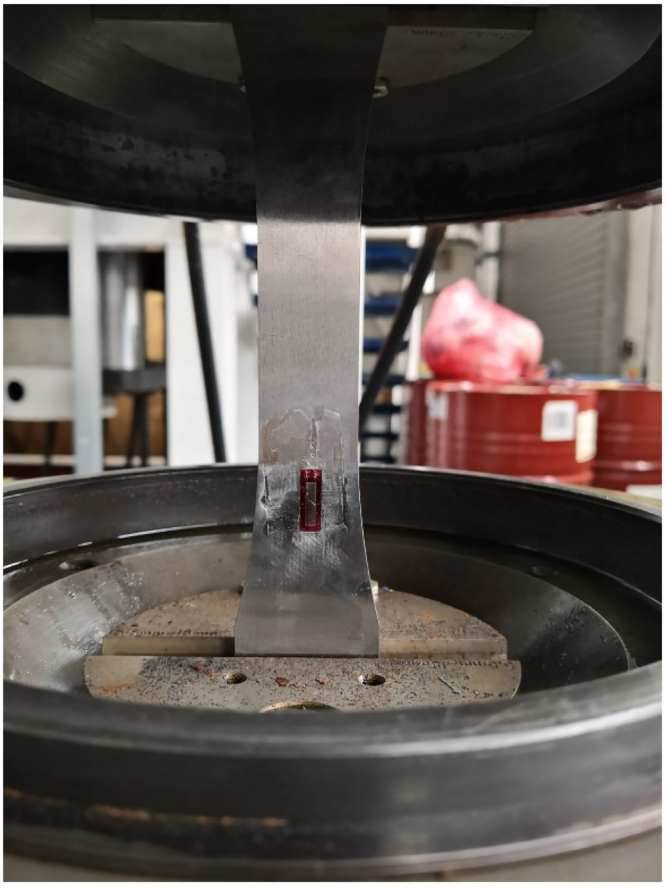

Fig. 3. Uniaxial fatigue specimen undergoing fatigue testing.

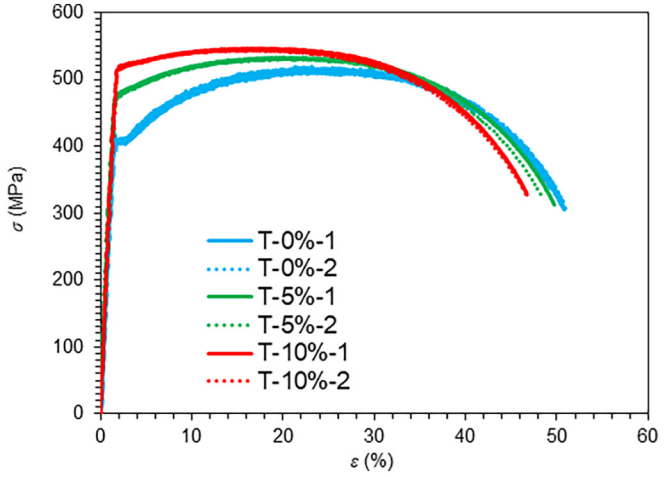

Fig. 2. Comparison of the tensile curves for 0%, 5% and 10% pre-strained materials.

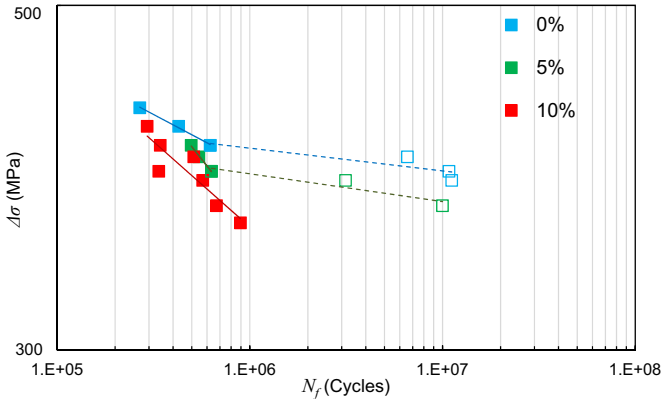

Fig. 4. Uniaxial fatigue data for 0%, 5% and 10% pre-strained materials.

Table 2
Power-law constants from bi-linear fits made to uniaxial fatigue data.

Pre-strain level (%)	$N_f \leq 6 \times 10^5$		$N_f > 6 \times 10^5$	
	$logA_1$	B_1	$logA_2$	B_2
0	45.50	−15.22	84.20	−68.35
5	22.33	−6.38	150.73	−55.87
10	29.28	−9.11	N/A	N/A

4.3. Tensile tests on fatigue damaged specimens

In order to evaluate the influence of prior fatigue damage on subsequent mechanical behaviour of the material, four interrupted fatigue tests were performed on 0% and 10% pre-strained materials, with two tests performed for each pre-strain level; denoted IF-0%-0.5 and IF-0%-0.8, and IF-10%-0.5 and IF-10%-0.8 for 0% and 10% material pre-strain levels, respectively, where IF stands for interrupted fatigue followed by the percentage of pre-straining whereas the final number identifies the level of fatigue damage (i.e. D). Similar to the tests performed in Section 4.2, the interrupted fatigue tests were also performed at the frequency of $f = 4$ Hz with the load ratio of $R = 0.1$. For comparison purposes, all four interrupted fatigue tests were performed at a fixed stress range of $\Delta\sigma = 406$ MPa at which a clear difference in the fatigue life can be observed in 0% and 10% pre-strained material (see Fig. 4). For each of the pre-strain levels, the first test was interrupted at the fatigue damage parameter of $D = 0.5$ while the second test was stopped at $D = 0.8$, according to Miner's rule (see the equation below) and by considering a constant stress amplitude loading condition of $\Delta\sigma = 406$ MPa (i.e. hence $k = 1$ in Eq. (2)). It is worth noting that in order to introduce the predefined values of fatigue damage in these tests, the required number of test cycles were calculated based on the total number of cycles for failure, N_f, at $\Delta\sigma = 406$ MPa for 0% and 10% pre-strain material states (see Fig. 4).

$$D = \sum_{i=1}^{k} \frac{n_i}{N_{f_i}} \tag{2}$$

Tensile tests were performed on interrupted fatigue samples and the results are presented in Fig. 5. Also included in this figure are the average tensile curves on 0% (denoted IF-0%-0) and 10% (denoted IF-10%-0) pre-strained materials without any pre-existing fatigue damage (i.e. $n = 0$ according to Eq. (2)). The mechanical properties obtained from the test on 0% and 10% pre-strained materials with different extent of fatigue damage are summarised in Table 3. As seen in Fig. 5 and Table 3, for 0% (i.e. AR) material state, a higher yield stress can be observed in interrupted fatigue tests compared to the undamaged material. Knowing that the applied stress level of $\Delta\sigma = 406$ has resulted in the maximum applied stress of $\sigma_{max} = 451$ MPa in these tests, the higher yield stress in the interrupted fatigue tests on the AR material state has occurred due to the hardening behaviour which takes place in the first fatigue cycle under a maximum stress level of greater than yield. On the other hand, knowing that the σ_{max} applied in interrupted fatigue tests on 10% pre-strained material is lower than the yield stress for this material state, there is no noticeable change observed in the yield stress of the fatigue damaged and undamaged pre-strained materials.

Table 3
Summary of mechanical properties obtained from specimens with different extent of pre-existing fatigue damage, for 0% and 10% pre-strained materials.

Specimen ID	Pre-strain level (%)	D	E (GPa)	σ_Y (MPa)	σ_{UTS} (MPa)	ε_f (%)
IF-0%-0	0	0	222	417	518	50.8
IF-0%-0.5	0	0.5	171	466	518	49.3
IF-0%-0.8	0	0.8	176	457	528	48.2
IF-10%-0	10	0	264	516	545	46.6
IF-10%-0.5	10	0.5	197	495	517	43.6
IF-10%-0.8	10	0.8	193	499	524	42.6

Also seen in Fig. 5 and Table 3 is that while the increase in σ_{UTS} and decrease in ε_f for the fatigue damaged AR specimens, compared to undamaged AR material, can be associated with material hardening in the first fatigue cycle (because $\sigma_{max} > \sigma_y$), the slight changes in σ_{UTS} and ε_f of 10% pre-strained specimens with different extent of fatigue damage can be considered negligible within the inherent experimental scatter. These results suggest that if uniaxial fatigue damage occurs at an applied maximum stress level of below yield, there will be no noticeable change in the mechanical properties of the material and the accumulation of fatigue damage has an insignificant effect on the macroscopic plastic properties of the material, including strain at failure which has been found to drop by less than 10% after the introduction of severe fatigue damage ($D = 0.8$) into the material.

4.4. Fatigue crack growth tests

Fatigue crack growth tests were performed on three AR specimens (denoted CT-0%-1–3), four 5% pre-strained specimens (denoted CT-5%-1–4) and four 10% pre-strained specimens (denoted CT-10%-1–4). As shown in Fig. 6, the cycle count and crack length were continuously monitored throughout the tests. Using this data, the fatigue crack growth rate, da/dN, was calculated via the incremental polynomial

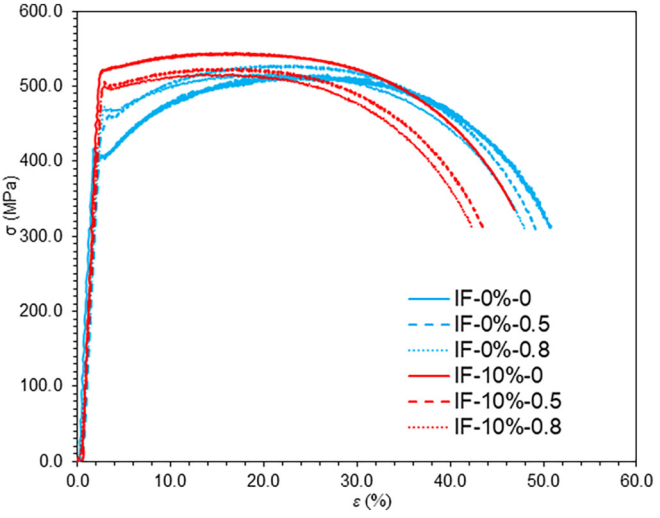

Fig. 5. Comparison of the tensile curves obtained from specimens with different extent of pre-existing fatigue damage, for 0% and 10% pre-strained materials.

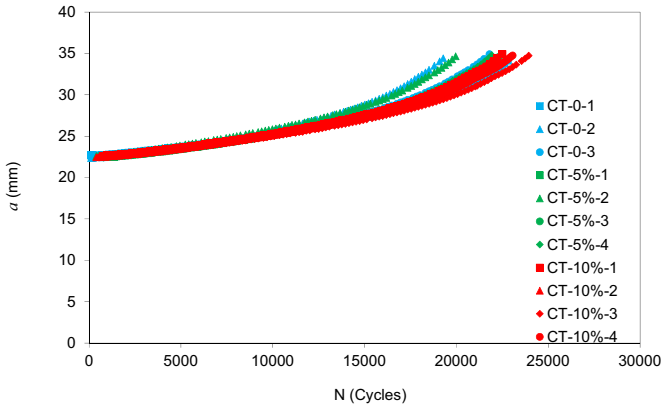

Fig. 6. a vs. N data obtained from fatigue crack growth tests for 0%, 5% and 10% pre-strain levels.

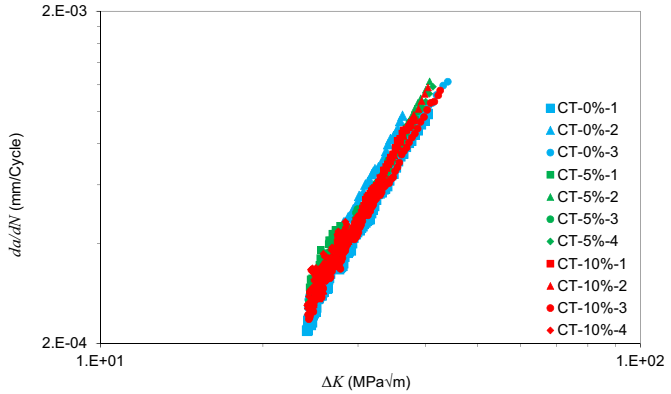

Fig. 7. Fatigue crack growth curves obtained from materials with 0%, 5% and 10% pre-strain levels.

technique and the results were correlated with the linear-elastic fracture mechanic parameter ΔK (i.e. difference between K_{max} and K_{min}) which can be calculated using the following equation:

$$\Delta K = Y\Delta\sigma\sqrt{\pi a} \quad (3)$$

where a is the crack length, $\Delta\sigma$ is the applied stress and Y is a dimensionless shape function, the solutions of which can be found in the literature [23,24]. Moreover, the fatigue crack growth data were analysed to quantify the power-law constants in the secondary fatigue region (also known as the Paris region) calculated following the equation below.

$$\frac{da}{dN} = C\Delta K^m \quad (4)$$

where C and m are known as the Paris law constants which can be identified using a power-law fit to the test data.

Table 4
Paris law constants for each specimen tested on 0%, 5% and 10% pre-strained materials.

Specimen ID	a_f-unloading compliance (mm)	a_f-fracture surface (mm)	a_f - % error	C (*10^{-8})	m
CT-0%-1	35.3	35.2	0.3	2.98	2.82
CT-0%-2	35.1	34.3	2.2	4.45	2.72
CT-0%-3	35.4	35.0	1.0	6.42	2.62
CT-5%-1	35.9	35.2	1.9	4.69	3.41
CT-5%-2	35.9	34.4	4.5	6.71	2.58
CT-5%-3	36.2	35.1	3.2	4.66	2.71
CT-5%-4	35.4	34.6	2.1	8.15	2.54
CT-10%-1	36.6	35.4	3.3	4.74	2.69
CT-10%-2	36.8	34.5	6.6	6.29	2.60
CT-10%-3	36.3	35.4	2.5	6.38	2.59
CT-10%-4	36.8	35.2	4.5	6.22	2.61

Table 5
Paris law constants based on mean and mean + 2SD curves for 0%, 5% and 10% material data sets.

Pre-strain level (%)	Mean curve			Standard deviation	Mean + 2SD	
	C	m	R^2		C	m
0	6.46×10^{-8}	2.59	0.925	0.025	8.77×10^{-8}	2.59
5	2.01×10^{-7}	2.27	0.951	0.019	2.52×10^{-7}	2.27
10	2.04×10^{-7}	2.25	0.978	0.017	2.39×10^{-7}	2.25

The correlation between the fatigue crack growth per cycle, da/dN, with ΔK is demonstrated in Fig. 7 and the Paris law constants for each data set are summarised in Table 4. As seen in Fig. 7 and Table 4, the experimental data sets obtained from materials with different pre-strain levels have been found to fall upon each other, indicating that plastic pre-straining doesn't have any noticeable impact on the fatigue crack growth behaviour of the material. This observation on S355 steel is consistent with the data reported on other types of steel in the literature [18,25]. This may be due to the fact that while material pre-straining may increase the yield behaviour of the material, it also decreases the strain at failure (as seen in Fig. 2). These behaviours may "cancel" each other out, resulting in similar fatigue crack growth rates between the AR and pre-strained material. In addition, curves for the a *vs.* N data for each pre-straining level from the fatigue crack growth testing have been included for reference. Included in Table 4 are the final crack length in the fatigue crack growth tests obtained using the unloading compliance data and optical measurements on the fracture surface. As seen in this table, the unloading compliance technique has been found to provide relatively high accuracy for estimation of the instantaneous crack length with the percentage of error found to be below 7%.

In order to evaluate the level of scatter in the fatigue crack growth data, for each material pre-straining level regression analysis has been conducted to work out the upper bound and lower bound trends by calculating and plotting the mean curve ±2 standard deviations (2SD). The comparison of the mean curve and mean ± 2SD trends for each material data set is shown in Fig. 8(a), (b) and (c) for 0%, 5% and 10% pre-strained material states, respectively, and the Paris law constants are summarised in Table 5. It can be seen in Fig. 8 and Table 5 that for each pre-straining level, there is a small SD in the test data indicating minimal scatter and good repeatability in the fatigue crack growth test data on AR and pre-strained specimens. Comparison of the results shown in Fig. 8 and Table 5 also shows that the Paris law constants obtained for the mean curve and the upper bound trend (mean + 2SD) are very similar for different pre-strain levels and the analysed trends fall on top of each other. This confirms that material pre-straining does not have any significant effect on the fatigue crack growth behaviour of the material. Finally included in Table 5 are the coefficients of determination, R^2, for the mean curves fitted to the data points obtained from

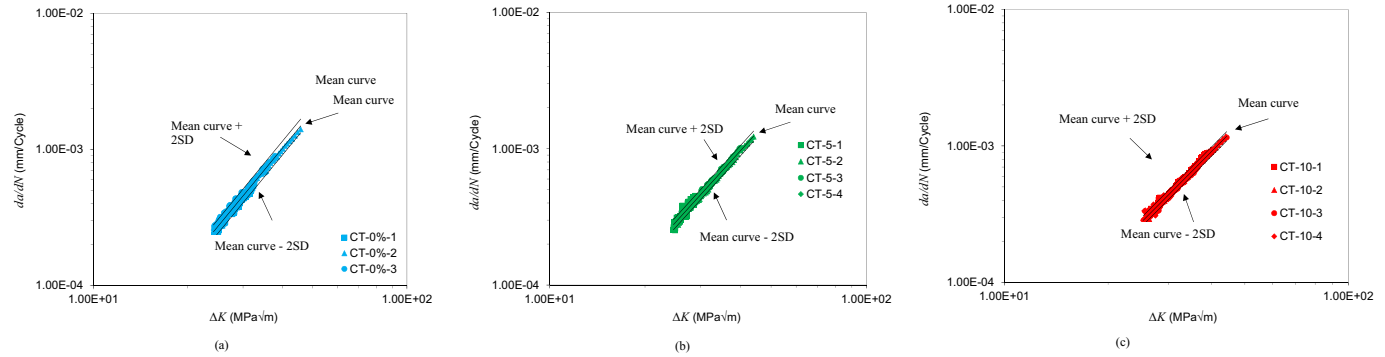

Fig. 8. Regression analysis of the fatigue crack growth data obtained from the tests on (a) 0%, (b) 5%, and (c) 10%, pre-strained material states.

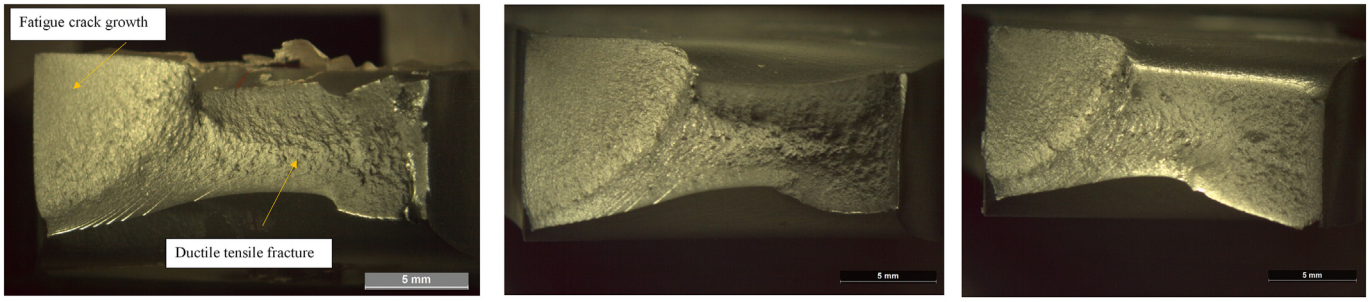

Fig. 9. Fracture surface of uniaxial fatigue samples with (a) 0%, (b) 5%, (c) 10% pre-strain.

each material pre-strain level. As seen in this table, the R^2 values for all three data sets are close to unity, confirming that for each pre-strain level the material's behaviour can be accurately described using the Paris law constants presented in Table 5.

4.5. Fractography

Fractography was conducted for all uniaxial fatigue and fatigue crack growth specimens post testing. Fig. 9(a), (b) and (c) correspond to the fracture surfaces of uniaxial fatigue specimens which were tested at a stress level corresponding to 86% of the ultimate tensile strength of S355, at pre-straining levels of 0%, 5% and 10% respectively. From the fracture surfaces, a smooth portion is visible where the fatigue crack growth would have initiated from the edge of the specimen due to edge effects. This was then followed by ductile tensile fracture of the specimens. This pattern is consistent throughout all fracture specimens; however, with increased pre-straining, the fracture surface appears to become smoother in the ductile tensile region; this may be due to the hardening behaviour of the material during pre-straining resulting in a less ductile fracture surface.

Fig. 10 shows the fractography images of the C(T) testing post fatigue crack growth testing. Three regions have been identified on the fracture surface during post mortem analysis. The smooth portion of the fracture surface shows the region of pre-fatigue cracking. This was followed by ductile crack extension before the specimen was broken via fast fracture. As there is uniformity in the fatigue crack region, this shows good alignment in the test set-up. Measurements from the fractographical assessment were taken and compared to those from the unloading compliance for comparison purposes.

5. Discussion

In order to assess the importance of material pre-straining in fatigue design and life assessment of offshore structures, the obtained uniaxial fatigue data from this study have been compared with the S-N fatigue design curves recommended for the base metal in various design codes and the results are shown in Fig. 11(a) [26–34]. It can be seen in this figure that the design curves across various standard bodies differ, with ISO 131819 being the most conservative, and IIW being the least conservative in the high stress region of the S-N curves. All design curves, for the air environment, indicate a change in slope once a certain number of cycles have elapsed, with most exhibiting a slope change at 10^7 cycles. An interesting point to note is that the fatigue curve of ISO 13819 is identical to BS 7608, up until the change in the slope at 10^7 cycles. It is believed that these curves may be somewhat conservative for the design of offshore structures, and thus, more optimised designs can be made by taking into account the level of conservatism in these design curves. Comparison of the uniaxial fatigue data on specimens with different levels of pre-strain with the S-N fatigue design curves available in various standards shows that although pre-straining has been found to have a significant effect on the fatigue life of the material, the level of conservatism in all design curves is high enough to suggest significantly lower number of cycles to failure for the pre-strained materials. However, if the design curves are to be revised in the future for reducing the level of excess conservatism, the influence of material pre-straining must be accounted for in the development of the revised curves.

Comparisons of the experimental test results with the mean and design curves from DNV have been presented in Fig. 11 (b). It can be seen in this figure that the obtained experimental data are not only falling ahead of the B1 design curve (mean – 2 standard deviation) but also

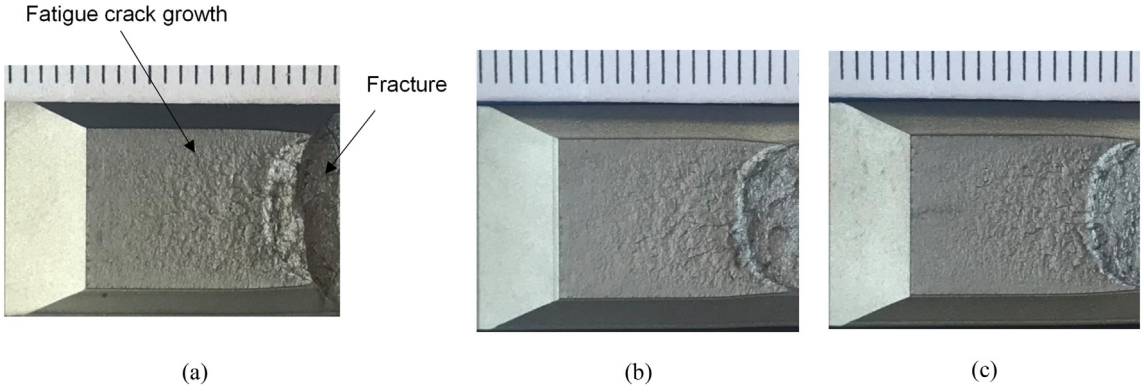

Fig. 10. Fracture surface of C(T) specimens with (a) 0%, (b) 5%, (c) 10% pre-strain (1 mm distance between division lines on the scale bar).

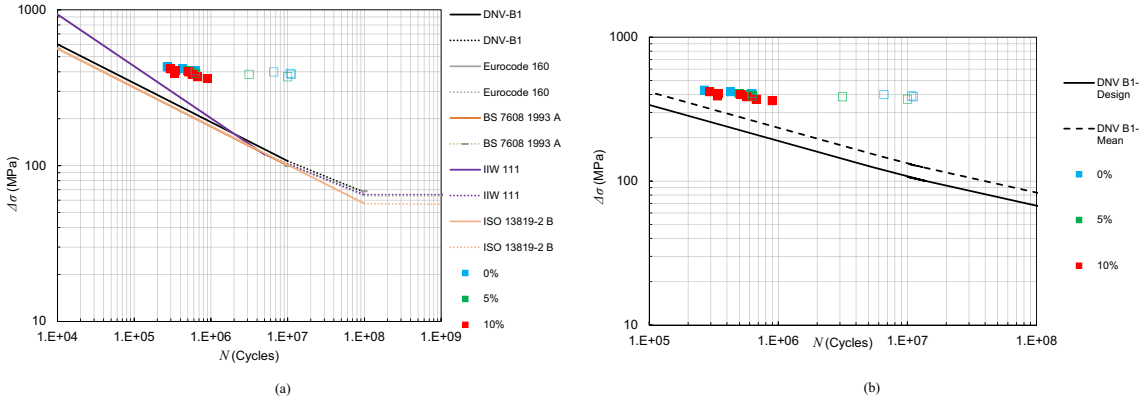

Fig. 11. (a) Comparison of the recommended S-N curves from standards with the test data obtained from the present study, (b) comparison of the experimental data to DNV B1 mean and design curves.

showing longer fatigue lives compared to the B1 mean curve taken from the DNV standard. This indicates that the proposed curves in the standards are conservative not only for the AR material but also for pre-strained material states. Having said that, further tests must be conducted on larger scale pre-strained specimens in future work to investigate the size effect on the fatigue behaviour of pre-strained materials.

As seen in Fig. 4 material pre-straining has been found to have a pronounced effect on the fatigue life at lower stress levels. It can be seen in Fig. 4 that the material pre-strained to a higher percentage exhibits a significantly lower number of cycles to failure. This indicates that the material with higher yield stress would have a lower fatigue life compared to lower yield stress materials. Knowing that the design curves provided in standards are given for a wide range of engineering materials with different values of yield stress, the experimental data presented in the current study show that selecting a material with a lower yield stress would result in fatigue lives which are significantly higher than those estimated by the design curves. In other words, considering that the design curves provided in standards are sufficiently conservative, selecting materials with higher yield stress would provide fatigue lives closer to those estimated by the design curves whereas the lower yield stress materials will have much longer fatigue lives. Although the present study was primarily focused on the pre-straining effects on the fatigue behaviour of S355, the results show that the fatigue life is sensitive to the yield stress of the material and material selection plays a big role in the actual fatigue life of engineering structures (e.g. monopiles and jackets) particularly at operational load levels (low stress levels).

The results presented in this study exhibited that material pre-straining has insignificant effects on the fatigue crack growth rate of S355 steel, therefore the pre-straining effect does not need to be accounted for in the life assessment of offshore structures. While a similar behaviour has been reported in this literature for pre-tensioning effects in pipe steels, it has been noticed that pre-compression may accelerate the fatigue crack growth rate of the material [18]. A study on pre-compressed SUH660 steel, a steel which is widely used in aircraft engines and gas turbines, also showed that the fatigue crack growth rates were accelerated compared to the AR material state [35]. Knowing that the extent of material pre-straining varies throughout the thickness of offshore wind monopiles, with tensile plastic strains on the exterior surface of the monopile and compressive strains on the interior [36], the observations in the literature may affect the way monopile defect assessment and inspection are conducted. However, further work may need to be conducted on the compressive pre-straining effects on the fatigue crack growth behaviour of S355.

The upper bound fatigue crack growth trends obtained from this study on 0%, 5% and 10% pre-strained material states have been compared with the recommended fatigue crack growth trend for base metal in BS 7910 [37] in Fig. 12. It can be seen in this figure that while pre-tensioning did not exhibit any noticeable effect on the crack growth behaviour of S355, the upper bound trends obtained from all three material data sets fall upon or just above the recommended curve from BS7910, using the simplified law, and well above the 2-stage law recommended in this standard. Therefore, the results obtained from this study suggest that while no consideration needs to be made to account for the influence of material pre-tensioning on the fatigue crack growth behaviour of the material, the fatigue crack growth rates in offshore structures might be under-predicted by using the recommended trends in BS7910. Further tests need to be conducted in future work to examine the fatigue crack growth rates in pre-compressed S355 material with the crack growth trends recommended in BS7910. Also more tests need to be conducted in future work on specimens with a larger thickness in order to investigate the size effects on the fatigue crack growth behaviour of pre-strained materials with a view to enhance the structural integrity assessment procedures for larger scale monopile structures.

6. Conclusions

Mechanical, uniaxial fatigue, interrupted fatigue and fatigue crack growth tests were conducted on S355GS + 10 structural steel with 0%, 5% and 10% tensile pre-strain states. From the experimental data it was observed that the fatigue life of S355 will significantly decrease with an increase in material pre-straining, particularly at lower stress levels where more than an order of magnitude reduction in fatigue life was

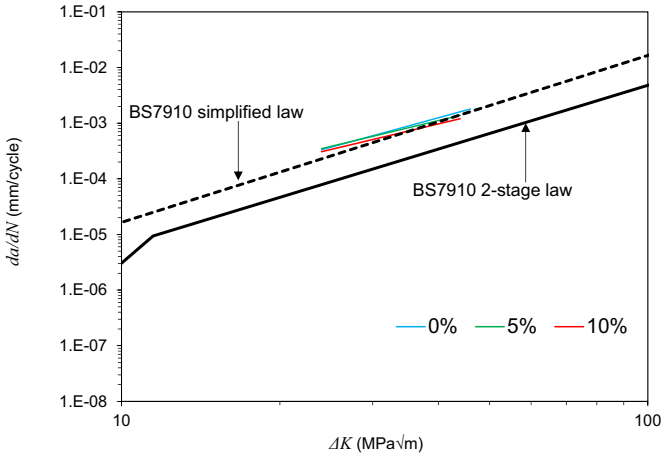

Fig. 12. Comparison of the recommended fatigue crack growth trends in BS7910 with the test data obtained from the present study.

found in the 10% pre-strained material. Bi-linear S-N curves, in log-log axes, were obtained for the 0% and 5% pre-strained material, with the slope change occurring at around 600,000 cycles. Further work needs to be conducted to determine the secondary slope for 10% pre-strained material at lower stress levels. The tensile tests on interrupted fatigue specimens revealed that if the applied stress level during fatigue cycles is less than the yield stress, fatigue damage has insignificant effects on the mechanical behaviour of the material. Finally, it was noted that material pre-tensioning had no impact on the fatigue crack propagation behaviour of S355; however, further tests must be conducted in future work to examine material pre-compression effects on the fatigue crack growth behaviour. While the S-N fatigue design curves in international standards provide conservative predictions of the fatigue life for the AR and pre-strained materials, the recommended trends in BS7910 standard may under-predict the fatigue crack growth rates in the AR an pre-strained materials. Therefore, greater care is required to account for material pre-straining effects on the fatigue design and life assessment of offshore structures with sufficient safety margins against failure.

Declaration of Competing Interest

The authors declare that they have no known competing financial interests or personal relationships that could have appeared to influence the work reported in this paper.

Acknowledgements

This work was supported by grant EP/L016303/1 for Cranfield, Oxford and Strathclyde Universities, Centre for Doctoral Training in Renewable Energy Marine Structures - REMS (http://www.rems-cdt.ac.uk/) from the UK Engineering and Physical Sciences Research Council (EPSRC).

References

[1] J. Velarde, C. Kramhøft, J.D. Sørensen, G. Zorzi, Fatigue reliability of large monopiles for offshore wind turbines, Int. J. Fatigue 134 (2020 May), 105487, https://doi.org/10.1016/2Fj.ijfatigue.2020.105487.
[2] M.D. Esteban, B. Couñago, J.S. López-Gutiérrez, V. Negro, F. Vellisco, Gravity based support structures for offshore wind turbine generators: review of the installation process, Ocean Eng. 110 (2015 Dec) 281–291, https://doi.org/10.1016/2Fj.oceaneng.2015.10.033.
[3] V. Negro, J.-S. López-Gutiérrez, M.D. Esteban, C. Matutano, Uncertainties in the design of support structures and foundations for offshore wind turbines, Renew. Energy 63 (2014 Mar) 125–132, https://doi.org/10.1016/2Fj.renene.2013.08.041.
[4] V. Igwemezie, A. Mehmanparast, A. Kolios, Current trend in offshore wind energy sector and material requirements for fatigue resistance improvement in large wind turbine support structures – a review, Renew. Sustain. Energy Rev. 101 (2019 Mar) 181–196, https://doi.org/10.1016/2Fj.rser.2018.11.002.
[5] A. Jacob, J. Oliveira, A. Mehmanparast, F. Hosseinzadeh, J. Kelleher, F. Berto, Residual stress measurements in offshore wind monopile weldments using neutron diffraction technique and contour method, Theor. Appl. Fract. Mech. 96 (June) (2018) 418–427, https://doi.org/10.1016/j.tafmec.2018.06.001.
[6] L. Orlando, Review of Design Procedures for Monopile Offshore Wind Structures, 2015.
[7] C. Pérez-Collazo, D. Greaves, G. Iglesias, A review of combined wave and offshore wind energy, Renew. Sustain. Energy Rev. 42 (2015 Feb) 141–153, https://doi.org/10.1016/2Fj.rser.2014.09.032.
[8] S. Anandavijayan, A. Mehmanparast, F. Brennan, A numerical analysis of the effects of manufacturing processes on material pre-strain in offshore wind monopiles, Procedia Structural Integrity, 2018.
[9] I. Lotsberg, Fatigue Design of Marine Structures, Cambridge University Press, 2016.
[10] A. Mehmanparast, C.M. Davies, D.W. Dean, K. Nikbin, Effects of plastic pre-straining level on the creep deformation, crack initiation and growth behaviour of 316H stainless steel, Int. J. Press Vessel. Pip. 141 (2016 May) 1–10, https://doi.org/10.1016/2Fj.ijpvp.2016.03.013.
[11] Baek J. Hyun, Kim Y. Pyo, Kim C. Man, Kim W. Sik, Seok C. Sung, Effects of pre-strain on the mechanical properties of API 5L X65 pipe, Mater. Sci. Eng. A 527 (6) (2010) 1473–1479.
[12] Y.H. Zhang, S.J. Maddox, S. Manteghi, Verification of Class B S-N curve for fatigue design of steel forgings, Int. J. Fatigue 92 (2016) 246–261, https://doi.org/10.1016/j.ijfatigue.2016.07.015.
[13] J. Kwon, D. Jeong, I. Choi, Y. Kim, N. Woo, S. Kim, Fatigue behavior of api x-80 steels, ASME Int. Mech. Eng. Congr. Expo. Proc. 3 (Parts A, B, and C) (2012) 1211–1218.
[14] A.K. Bhargava, C. Sharma, Mechanical Behaviour of Materials, 2011.
[15] A.M.P. de Jesus, R. Matos, B.F.C. Fontoura, C. Rebelo, L.S. da Silva, M. Veljkovic, A comparison of the fatigue behavior between S355 and S690 steel grades, J. Constr. Steel Res. 79 (2012 Dec) 140–150, https://doi.org/10.1016/2Fj.jcsr.2012.07.021.
[16] D. Forni, B. Chiaia, E. Cadoni, High strain rate response of S355 at high temperatures, Mater. Des. 94 (2016 Mar) 467–478, https://doi.org/10.1016/2Fj.matdes.2015.12.160.
[17] R. Pawliczek, M. Prażmowski, Study on material property changes of mild steel S355 caused by block loads with varying mean stress, Int. J. Fatigue 80 (2015 Nov) 171–177, https://doi.org/10.1016/2Fj.ijfatigue.2015.05.019.
[18] N. Hagiwara, T. Masuda, N. Oguchi, Effects of prestrain on fracture toughness and fatigue-crack growth of line pipe steels, J. Press. Vessel Technol. 123 (3) (2001 Apr) 355–361, https://doi.org/10.1115/2F1.1379531.
[19] Y.C. Chiou, J.K. Yang, The effects of pre-deformation on the subsequent fatigue behaviors of SUS 430 stainless steel in load-control, Int. J. Solids Struct. 49 (23–24) (2012) 3263–3268, https://doi.org/10.1016/j.ijsolstr.2012.06.023.
[20] J.C. Le Roux, S. Taheri, J.P. Sermage, J. Colin, A. Fatemi, Cyclic deformation and fatigue behaviors of stainless steel 304L including mean stress and pre-straining effects, Am. Soc. Mech. Eng. Press. Vessel Pip. Div. 3 (2008) 411–420.
[21] Y.B. Guo, H.C. Ho, K.F. Chung, A.Y. Elghazouli, Cyclic deformation characteristics of S355 and S690 steels under different loading protocols, Eng. Struct. 221 (June) (2020).
[22] D. Forni, B. Chiaia, E. Cadoni, Strain rate behaviour in tension of S355 steel: base for progressive collapse analysis, Eng. Struct. 119 (2016 Jul) 164–173, https://doi.org/10.1016/2Fj.engstruct.2016.04.013.
[23] ASTM E647−13, Standard test method for measurement of fatigue crack growth rates, Am. Soc. Test Mater. (2014) 1–50.
[24] A. Mehmanparast, F. Brennan, I. Tavares, Fatigue crack growth rates for offshore wind monopile weldments in air and seawater: {SLIC} inter-laboratory test results, Mater Des. 114 (2017 Jan) 494–504, https://doi.org/10.1016/2Fj.matdes.2016.10.070.
[25] A. Mehmanparast, The Influence of Inelastic Damage on Creep, Fatigue and Fracture Toughness, Dep. Mech. Eng, 2012 PhD(September).
[26] R. Brandi, P. Rossetto, Fatigue design of offshore structures, Weld. Int. 1 (12) (1987) 1155–1161.
[27] H E U R O P E a N N I O N. 2011(1) (2005).
[28] The British Standards Institution. BS 7608 2014 (preview.pdf).
[29] A. Hobbacher, IIW Document IIW-1823-07 Fatigue Design of Welded, 2008.
[30] HSE, Offshore Technology Report 2001/083 - Comparison of Fatigue Provisions in Codes and Standards, http://www.hse.gov.uk/research/otopdf/2001/oto01083.pdf 2002.
[31] BSI, BS 7608: Code of practice for fatigue design and assessment of steel structures, 1993.
[32] ISO, ISO 13819-2: Petroleum and Natural Gas Industries - Offshore Structures - Part 2: Fixed Steel Structures, 1999.
[33] HSE, Offshore Installations: Guidance on Design, Construction and Certification, 1993.
[34] NORSOK, Design of Steel Structures, 1998.
[35] H. Wu, S. Hamada, H. Noguchi, Pre-strain effect on fatigue strength characteristics of SUH660 plain specimens, Int. J. Fatigue 55 (2013) 291–298, https://doi.org/10.1016/j.ijfatigue.2013.06.021.
[36] Anandavijayan S, Mehmanparast A, Brennan F. A numerical analysis of the effects of manufacturing processes on material pre-strain in offshore wind monopiles. Proc. Struct. Integr. 2018;13:953–8. doi:10.1016/2Fj.prostr.2018.12.178.
[37] BS 7910, BSI Standards Publication Guide to methods for assessing the acceptability of flaws in metallic structures, BSI Stand Publ., UK, 2015 490.